A&A 659, A122 (2022)
https://doi.org/10.1051/0004-6361/202142563

Astronomy & Astrophysics

Metallicity of the globular cluster NGC 6388 based on high-resolution spectra of more than 160 giant stars⋆,⋆⋆

Eugenio Carretta and Angela Bragaglia

INAF-Osservatorio di Astrofisica e Scienza dello Spazio di Bologna, via Gobetti 93/3, 40129 Bologna, Italy
e-mail: eugenio.carretta@inaf.it, angela.bragaglia@inaf.it

Received 2 November 2021 / Accepted 22 November 2021

ABSTRACT

NGC 6388 is one of the most massive Galactic globular clusters (GC) and it is an old, metal-rich Galactic bulge cluster. By exploiting previous spectroscopic observations, we were able to bypass the uncertainties in membership related to the contamination from strong field stars. We present the abundance analysis of 12 new giant stars with UVES spectra and 150 giants with GIRAFFE spectra acquired at the ESO-VLT. We derived radial velocities, atmospheric parameters, and iron abundances for all the stars. When combined with the previous data, we obtained a grand total of 185 stars homogeneously analysed in NGC 6388 from high-resolution spectroscopy. The average radial velocity of the 185 stars is 81.2 ± 0.7, rms 9.4 km s^{-1}. We obtained an average metallicity [Fe/H] = −0.480 dex, rms = 0.045 dex (35 stars), and [Fe/H] = −0.488 dex, rms = 0.040 dex (150 stars) from the UVES and GIRAFFE samples, respectively. Comparing these values to the internal errors in abundance, we excluded the presence of a significant intrinsic metallicity spread within the cluster. Since about a third of giants in NGC 6388 is claimed to belong to the 'anomalous red giants' in the HST pseudo-colour map defining the so-called type-II GCs, we conclude that either enhanced metallicity is not a necessary requisite to explain this classification (as also suggested by the null iron spread for NGC 362) or NGC 6388 is not a type-II globular cluster.

Key words. stars: abundances – stars: atmospheres – stars: Population II – globular clusters: general – globular clusters: individual: NGC 6388

1. Introduction

The metal-rich and massive bulge globular cluster (GC) NGC 6388 ([Fe/H] = −0.44[1], Carretta et al. 2007a; M_V = −9.41 mag, Harris 1996, 2010 web edition) certainly deserves attention due to its many peculiar features: (a) beside the red horizontal branch (HB) typical of old, metal-rich GCs, NGC 6388 shows an extended blue HB, namely, we see the second parameter at work within the same cluster. The He enrichment in the second generation stars (as suggested by D'Antona & Caloi 2004; see also Gratton et al. 2010) is likely the explanation, as shown by NGC 6388 participating to the strong correlation between extension of the Na-O anti-correlation and maximum temperature on the HB (Carretta et al. 2007b); (b) NGC 6388 is a local counterpart of old, metal-rich populations found in distant elliptical galaxies, and its relevant population of hot HB stars is a likely contributor to the UV-upturn phenomenon (e.g., Yi et al. 1998); (c) NGC 6388 is a pivotal cluster to probe the existence of intermediate-mass black holes (IMBH 10^3−10^4 $M_\odot$) whose evidence in this GC is controversial (Lanzoni et al. 2013, hereinafter L13; Lützgendorf et al. 2015); (d) NGC 6388 has been classified, on the basis of HST photometry pseudo-colours (the so-called 'chromosome map', ChM, Milone et al. 2017) as an example of a sub-class dubbed type-II GCs, that is, GCs showing not only a separation between putative first and second populations, but also an additional 'anomalous' population. According to Milone et al. (2017), a type-II GC is characterised by at least one of the following features: presence of separate subgiant and red giant branches (SGB, RGB), variation in C+N+O content (and/or age), and enhanced heavy elements abundances (iron and neutron-capture elements).

In our project on NGC 6388, we concentrate on the last point, spectroscopically studying a large sample of cluster stars. We successfully bypassed the problem of the heavy field contamination affecting this GC by exploiting a large mass of spectroscopic data acquired for various purposes and contained in the ESO archive. By forecasting high probability members from their radial velocity, we were able to derive an homogeneous chemical characterisation of a large sample of cluster stars using high resolution spectroscopy of individual targets. We tackle the problem of a possible metallicity dispersion, which seems to be a common requisite for so called type-II GCs. We present here the full set of atmospheric parameters (temperature, gravity, and metallicity) while abundances of light and heavy elements will be presented in a forthcoming paper.

NGC 6388 is generally classified as a bulge GC, not only based on its current location in the Galaxy (Galactocentric distance 3.1 kpc, 1.2 kpc below the Galactic plane, Harris 1996, 2010 edition) but also because it follows an highly bound orbit, with an apocenter at less than 3.5 kpc (e.g., Massari et al. 2019). It is an old GC (Ortolani et al. 1995) and its high metallicity places the cluster among a near uniform old age group in the age-metallicity relation (AMR). Based on the location on

⋆ Full Tables 2 and 3 are only available at the CDS via anonymous ftp to cdsarc.u-strasbg.fr (130.79.128.5) or via http://cdsarc.u-strasbg.fr/viz-bin/cat/J/A+A/659/A122

⋆⋆ Based on observations collected at ESO telescopes under programmes 073.D-0211, and 073.D-0760, 381.D-0329, 095.D-0834, 099.D-0047.

[1] We adopt the usual spectroscopic notation, i.e. [X] = $\log(X)_{star}$ − $\log(X)_\odot$ for any abundance quantity X, and $\log \epsilon(X) = \log(N_X/N_H) + 12.0$ for absolute number density abundances.

Article published by EDP Sciences

the AMR and in the integral of motion space, Forbes (2020) assigns NGC 6388 to the in situ group of Milky Way GCs, confirming the classification by Massari et al. (2019; however, see Myeong et al. 2019 and Minelli et al. 2021 for a different view). All this confirms the nature of the cluster as an object of interest that merits an in-depth study with regard to both its chemical and astrometric properties.

The existence of a possible metallicity spread in NGC 6388 is a controversial topic. From an apparent qualitative resemblance of its colour-magnitude diagram (CMD) with that of ω Cen (NGC 5139), Piotto et al. (1997) raised the suspicion of a metallicity spread to explain both the spread in colour of the RGB and the peculiar HB of NGC 6388. However, Raimondo et al. (2002) found that a broad spread in metallicity abundance could not be reconciled with the CMD features. From Washington photometry, Hughes et al. (2007) were able to put an upper limit to the metallicity spread, estimated to be less than 0.2 dex, supporting the abundance analysis of eight cool giants by Wallerstein et al. (2007), who derived a root mean square (rms) scatter of 0.1 dex.

Ours was the first study to obtain the spectra for many stars in NGC 6388, using FLAMES (Carretta et al. 2007a, 2009b), however, before *Gaia* and other spectroscopic surveys of this cluster, the pointing of potential targets was perforce a shot in the dark. In fact, NGC 6388 is strongly contaminated by both disk and bulge stars. While the use of precise astrometry could have helped the target selection even in this very crowded and difficult field, the spectra were acquired long before *Gaia* Data Release 2 (which went public on April 2018) and we were able to measure Fe, O, and Na only in 32 member stars – almost the lowest number in our FLAMES survey of GCs (Carretta et al. 2006, 2009a,b, 2010a). This clearly called for a corroboration via more robust statistics.

We then decided to take advantage of the huge potential of the ESO archive. The first results based only on UVES spectra of 24 new member stars were presented in Carretta & Bragaglia (2018). We measured Fe and 15 other elements, finding no spread in metallicity. We also confirmed the normal light elements' anti-correlations that were found found in all GCs, with clearly defined groups of primordial, intermediate, and extreme composition stars (P, I, and E as defined in Carretta et al. 2009b). However, if part of the cluster population is distinct by some difference in abundance, the fraction can be quite small. For instance, in NGC 362 Carretta et al. (2013) found a secondary giant branch containing only about 6% of RGB stars that were more Ba-rich than the bulk of normal RGB giants.

Hence, it is important to analyse as large samples as possible. In particular, L13 presented metallicities for about 280 NGC 6388 giants, partly from direct analyses of iron equivalent widths (EWs) and partly from the infrared calcium triplet (CaT) method. They did not find a significant metallicity spread, but the detailed abundance analysis was not published. Recently, the discussion on a possible spread in metal abundance for NGC 6388 was resumed following the studies by Mészáros et al. (2020, hereinafter M20) from infrared APOGEE spectra and Husser et al. (2020, from now H20) from low-resolution MUSE spectra.

Here, we present the whole sample of archival and new data to give a clear-cut answer to the issue of the intrinsic metallicity spread (or the lack of it) in NGC 6388, exploiting a large sample of stars with high resolution spectra analysed in the most homogeneous way. We also provide abundances of iron for individual stars as well as the atmospheric parameters derived on the same scale as in our previous works on more than 25 GCs. These values will be used in a forthcoming paper devoted to a full exploration of the chemical characterisation of multiple population in NGC 6388, their link with the dynamics, the clues from chemistry on the origin of this GCs, and other issues. The present paper is organised as follows: the data sets are described in Sect. 2 and the analysis in Sect. 3. Results on the metallicity distribution and a comparison with the literature data are presented in Sect. 4. A discussion of NGC 6388 in the context of type-II GCs is given in Sect. 5. Finally, we present a summary in Sect. 6.

2. Sample selection, observations, and prior data

The choice of targets in our latest observing programme (099.D-0047) was helped by the existing data sets available in the ESO archive describing membership. This was our starting point and a key step to avoid wasting telescope time on contaminating field stars whose densities are very high toward NGC 6388 – an issue that plagued the performance of our original programme (073.D-0211).

To ensure an optimal return from the observing time spent on targets, we considered three main data sets present in the ESO archive of advanced data products (see Table 1). All spectra considered were acquired with FLAMES (Pasquini et al. 2000). There are 539 GIRAFFE spectra taken with the high-resolution setup HR21 (R = 18 000, wavelength coverage ~8480−9000 Å) for 398 stars from L13 (ESO programme 381.D-0329). From ESO programme 95.D-0834 (P.I. Henault-Brunet, hereinafter, the H-B sample) we retrieved 1112 GIRAFFE HR13 spectra (R = 24 000, spectral range ~6115−6400 Å) for 113 stars. Finally, from the programme 073.D-0760 (P.I. Catelan; hereinafter CAT sample), we found 113 GIRAFFE HR13 spectra.

To select member stars we adopted the range in radial velocity (RV) as given in L13, whose large sample was designed to study the velocity dispersion in NGC 6388. Restricting the RVs to the interval 50–110 km s^{-1} (as in L13), we obtained 276, 65, and 53 candidate member stars from L13, H-B, and CAT, respectively. This was the original pool from which to cull our final targets.

A posteriori, we cross-matched our total 185 targets with the table of membership probability by Vasiliev & Baumgardt (2021), based on *Gaia* Early Data Release 3 results (Gaia Collaboration 2021), We found 176 stars in common. For 90% of them, the astrometric membership probability is in agreement with the one based on RV: 152 stars out of 176 have probability larger than 0.9, and 7 more have probability between 0.5 and 0.9. Given the different methods and the not-yet-optimal performance of *Gaia* in dense fields, we deem this a successful comparison.

The criteria for configuring the pointings were driven by the available archive material as well as by our main purposes: to derive a clear-cut answer on the intrinsic metallicity distribution in NGC 6388 and to obtain a detailed chemical characterisation of the multiple stellar populations hosted in this GC. Our observing strategy was then set as follows. For the stars observed only with HR21, we can derive Al abundances, so we need to complement them with HR13 spectra to also derive O, Na, and Mg, alongside the metallicity and atmospheric parameters, in a homogeneous way. For stars with HR13 spectra only, we wanted to add HR21 spectra to also derive Al abundances to obtain the complete set of proton-capture elements involved in (anti-)correlations defining multiple stellar populations in GCs.

Taking the sample by L13 as the main source of targets, we counter-identified the 276 member stars with HR21 spectra with

Table 1. Proprietary and archive data used in this paper.

Programme	Sample	Obs date	Obs time	Setups
073.D-0211 (PI Carretta)	C09	May to July 2004	19.6 h	HR11, HR13, U580
099.D-0047 (PI Carretta)	us	April to August 2017	11.9 h	HR13, HR21, U580
073.D-0760 (PI Catelan)	CAT	July 2004	3 h	HR13, U580
381.D-0329 (PI Lanzoni)	L13	June to July 2008	3 h	HR21, U580
095.D-0834 (PI Henault-Brunet)	H-B	June 2015	3.8 h	HR13, U580

Notes. Wavelength coverage – HR11: 5597-5840; HR13: 6120-6405; HR21: 8484-9001; U580: 4800–6800 Å. The GIRAFFE setups prior and later than February 2015 have slightly different resolutions, see data on ESO webpages.

the photometry obtained with the Wide Field Imager (WFI) at the ESO 2.2m telescope, which we used for our previous analysis and described in Carretta et al. (2007a). We selected only stars with $V < 16.25$ to avoid excessively long exposure times; to these, we added stars from the H-B sample with low signal-to-noise ratios (S/N) in their HR13 spectra. Ten one-hour exposures were obtained in Service Mode by ESO personnel in 2017 (see Table 1).

As a complementary data set, we considered stars that had HR13 observations but lacked HR21 spectra to define a second configuration for the observations with the HR21 setup. Two exposures (3160 s each) were obtained on 24 and 28 July 2017.

Finally, FLAMES/UVES fibres were put on the brightest giants to obtain the full pattern of the chemical composition, from the lightest to the heaviest (neutron-capture) species (using the 580 setup). During the previously described exposures, we then observed 12 member stars at $R \sim 47\,000$ and with wavelength coverage from about 4800 to 6800 Å.

The observations with the setup HR13 were combined (when feasible) with the archival data or spectra for the limited sample of stars used in Carretta et al. (2009b). From the latter, we only considered the HR13 setup, to achieve the maximum possible degree of homogeneity. Most of the Fe I and Fe II lines to derive the metal abundance fall in the spectral range of HR13 spectra, as well as transitions of the O, Mg, Si, Ca, and Sc species. Neglecting the HR11 setup, where the Na doublet at 5682–88 Å lies, has no consequences, as the weaker lines of Na at 6154–60 Å are strong enough to secure precise abundances of this element at the high metallicity of NGC 6388.

In Table 2, we list the relevant information to identify all stars in our sample. Since the naming convention is different in each sub-sample (L13, CAT, H-B) we used our unique code (Col. 1) to identify each star. The coordinates RA and Dec easily allow the cross-identification among all the sub-samples. The source for the spectra used for each stars and the estimated S/N ratio are listed in Cols. 2 and 3. We also provide in Table 2 optical magnitudes obtained with the WFI (see Carretta et al. 2007a). Near infrared K magnitudes are from 2MASS (Skrutskie et al. 2006). A V magnitude derived from a V versus K calibration based on all stars with both magnitudes available was assigned to stars not present in the WFI photometry (flag=0 in the last column of Table 2).

The total sample of the present work includes 150 stars with GIRAFFE HR13 spectra and 12 with UVES spectra. To it, we can also add the 24 stars with UVES spectra homogeneously analysed in Carretta & Bragaglia (2018). Our final sample in NGC 6388 is then composed of 185 giants (star n63n in the present study is also star A04 in Carretta & Bragaglia 2018).

Differently from other GCs studied in our FLAMES survey, where we selected stars lying near the RGB ridge line, in NGC 6388 we followed selection criteria based on RV, so that the final sample contains small sub-samples of stars in other evolutionary stages. From the position in the CMDs, we identified 17 stars on the asymptotic giant branch (AGB) and 10 stars on the red horizontal branch (RHB). Together with the bulk of RGB stars in our sample, they are plotted on the $K, V-K$ colour magnitude diagram in Fig. 1.

The histogram of the RV (measured using the IRAF task *rvidlines*) of these 185 stars is shown in Fig. 2, together with the distribution of non members from the archive data and our original observations. The average radial velocity of the 185 stars considered cluster members is 81.2 ± 0.7, rms 9.4 km s^{-1}. Finally, we cross-matched our targets with the table of individual stellar radial velocities of stars in the fields of globular clusters available on Holger Baumgardt's webpage[2], finding 159 stars in common. A plot of the differences in RV is shown in Fig. 3, where two stars with differences larger than 10 km s^{-1} are omitted. Without them, the average offset is -1.72 (rms 0.98) km s^{-1}. Star l63p154, in particular, shows a difference +68.11 km s^{-1} and a possible explanation is that the star is a binary. Our observations, taken in a short time interval, do not display significant changes around +85 km s^{-1}; however, the value listed at Baumgardt's web page is 17.46 km s^{-1} while L13 have 2.8 km s^{-1}. A more detailed comparison is outside the main goal of our paper and we do not proceed further.

3. Abundance analysis and error budget

The derivation of metallicity and of atmospheric parameters for all stars in our sample are based on EWs of neutral and singly ionised iron lines. We measured EWs with the package ROSA (Gratton 1988) as described in Bragaglia et al. (2001). The line list is the same used in all the papers of our FLAMES survey to study the Na-O anti-correlation in GCs (presented in Carretta et al. 2006, 2010a). The solar reference abundances are from Gratton et al. (2003). We recall here that the solar value for iron (the only element discussed in the present paper) is log ϵ(Fe) = 7.54 for Fe I and 7.49 for Fe II. For comparison, other reference solar values for iron commonly used are, for instance, 7.50 (Grevesse & Sauval 1998), 7.45 (Grevesse et al. 2007), and 7.50 (Asplund et al. 2009).

The EWs measured on the GIRAFFE HR13 spectra were converted to the scale of EWs measured on high resolution UVES spectra using lines measured on stars observed with both spectrographs (four, five, and four stars in our new observations and from CAT and H-B samples, respectively). UVES spectra are taken from Carretta et al. (2007a), Carretta & Bragaglia (2018) and from the present work.

[2] https://people.smp.uq.edu.au/HolgerBaumgardt/globular/

Table 2. Names, original sample, coordinates, magnitudes, and radial velocities of program stars.

Star	Sample	S/N	RA	Dec	V(wfi)	B(wfi)	K(2ma)	wfi	RV
n63a	UVES	30	264.080826	−44.733165	14.968	16.511	10.078	1	75.54
n63b	UVES	30	264.089261	−44.728379	15.18		9.733	0	62.66
n63c	UVES	40	264.096031	−44.745935	14.99	16.995	9.618	1	85.77
n63d	UVES	50	264.073095	−44.744597	14.804	16.616	9.694	1	88.10
n63e	UVES	50	264.094481	−44.75657	15.188	17.097	10.394	1	105.47
n63f	UVES	60	264.045909	−44.750423	15.14	17.009	10.381	1	81.56
n63g	UVES	40	264.143672	−44.71806	15.252	17.384	9.57	1	72.48
n63h	UVES	50	264.129650	−44.72916	15.071	17.04	9.954	1	79.72
n63i	UVES	65	264.069704	−44.706032	15.161	17.095	10.218	1	71.44
n63l	UVES	45	264.047492	−44.766651	15.233	17.033	10.707	1	76.80
n63m	UVES	55	264.215366	−44.728741	15.18		10.115	0	80.39
n63n	UVES	30	264.033217	−44.736818	14.757	16.678	9.731	1	83.65
l63p001	H-B	60	263.972502	−44.765736	16.832	18.329	13.366	1	89.83
l63p002	H-B	49	263.863453	−44.752747	17.064	18.469	13.745	1	96.12
l63p003	C09	90	263.952259	−44.750931	17.701	19.061	14.457	1	87.29
l63p004	H-B	58	263.940325	−44.717125	16.701	18.139	13.21	1	83.73
l63p006	us	20	263.962607	−44.686058	17.717	19.106	14.212	1	74.61
l63p007	H-B	134	263.958385	−44.677128	15.279	17.180	10.68	1	92.17
l63p008	H-B	52	263.869447	−44.646568	16.701	18.291	12.676	1	68.01
l63p010	us	45	264.168471	−44.787724	17.62	18.981		1	79.07
l63p011	C09	120	264.016210	−44.786659	16.574	18.029	12.934	1	79.13
l63p012	H-B	70	264.024788	−44.783100	16.48	17.955	12.756	1	76.54
l63p013	H-B	53	264.088182	−44.782795	17.053	18.429	13.622	1	67.41
l63p014	C09	120	264.090260	−44.774242	17.556	18.876	14.408	1	74.66
l63p015	CAT+H-B	112	264.124013	−44.766060	15.985	17.613	11.931	1	82.63
l63p017	H-B	55	264.163561	−44.733860	16.944	18.423	13.195	1	83.42
l63p018	C09	130	264.163546	−44.733825	16.582	18.143		1	88.95

Notes. The complete table is available at CDS, Strasbourg. Star n63n is star A04 in Carretta & Bragaglia (2018). Sample: us = this work, new observations, H-B =Henault-Brunet, C09 = Carretta et al. (2009b) CAT = Catelan, L13 = Lanzoni et al. (2013). WFI = 1 (0) if the star is present (absent) in the WFI catalogue (see text).

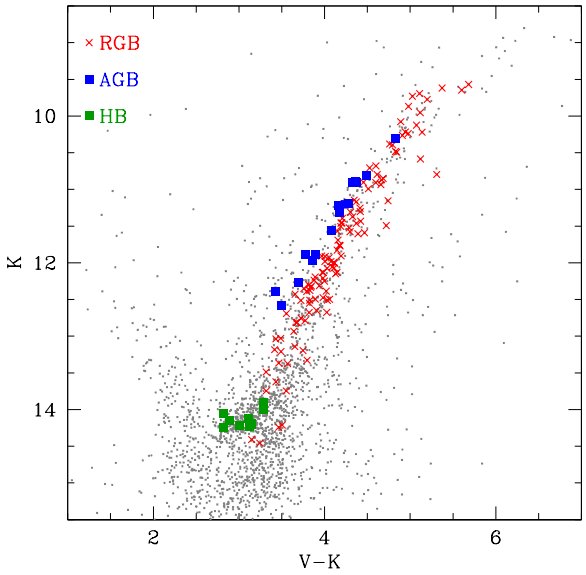

Fig. 1. $K, V-K$ colour magnitude diagram of NGC 6388 from WFI and 2MASS photometry (grey dots). Stars observed with spectroscopy in the present work are labelled and indicated with larger symbols: red crosses, blue squares, and green squares for RGB, AGB, and RHB stars, respectively.

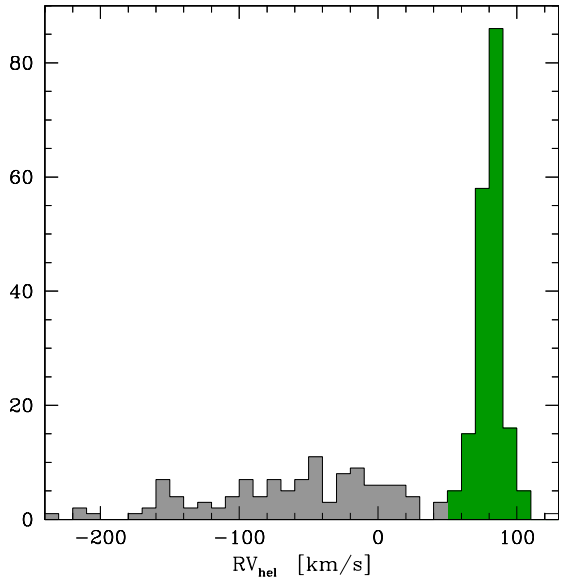

Fig. 2. Histogram of the RV values, from this paper, Carretta et al. (2007a; 2009b), and Carretta & Bragaglia (2018). We show in green the candidate members and in grey the non members (one star, at large positive RV, is not shown).

The procedure to derive the atmospheric parameters is the same adopted for the other works in our FLAMES survey, so that the derived abundances are on a strictly homogeneous scale. Effective temperatures ($T_{\rm eff}$) were obtained from a

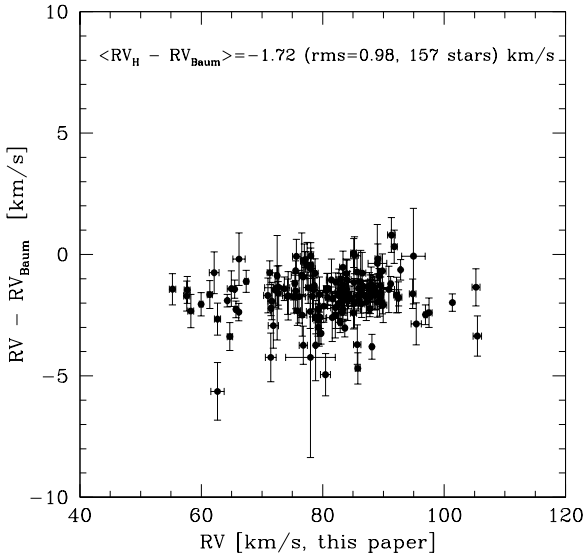

Fig. 3. Difference in RV between our sample and the data at the Baumgardt website. Two outliers, with large ΔRV values, are omitted (see text) in the plot.

calibration between magnitudes and values of $T_{\rm eff}$ from dereddened $V-K$ colours. The latter temperatures were derived from the Alonso et al. (1999, 2001) relation. For NGC 6388 we used K magnitudes. that are less affected by reddening than $V-K$ colours. The rationale for this approach, aimed at reducing the star-to-star errors, is discussed in detail in Gratton et al. (2007) for NGC 6441, another bulge cluster heavily affected by extinction.

Surface gravities were obtained from the above temperatures, adopting distance modulus $(m-M)_V = 16.14$ and reddening $E(B-V) = 0.37$ from Harris (1996, 2010 on line edition), bolometric corrections from Alonso et al. (1999), masses of $0.90\,M_\odot$ and $M_{\rm bol,\odot} = 4.75$. The relations $E(V-K) = 2.75E(B-V)$, $A_V = 3.1E(B-V)$, and $A_K = 0.353E(B-V)$ are taken from Cardelli et al. (1989).

We minimised the slope of the relation between abundances of Fe I and expected line strength (see Magain 1984) to derive the values of the microturbulent velocity v_t. From the Kurucz (1993) grid, we selected the model whose abundance was equal to the average abundances from Fe I lines. Adopted atmospheric parameters and derived abundances of Fe are listed in Table 3 (only an excerpt is shown, the entire table is available at CDS). The listed rms scatter is the line-to-line scatter. On average, we measured 100 Fe I and 13 Fe II lines from the UVES spectra and 20 Fe I and 3 Fe II from the GIRAFFE HR13 spectra.

We estimated star-to-star errors due to uncertainties in the adopted atmospheric parameters and in EW measurement using our usual procedure, amply described in Carretta et al. (2009a) for UVES and Carretta et al. (2009b) for GIRAFFE. The results for the present work are tabulated in Tables 4 and 5 for errors in iron abundances derived from UVES and GIRAFFE spectra, respectively.

In the main body of these tables, we list the sensitivities of abundance ratios [Fe/H] to changes in the atmospheric parameters, obtained by changing each of the parameters at the time for all stars, then taking the average. The amount of the variation is listed in the first row of each table. In the second and third row, the star-to-star (internal) errors and the systematic errors in each parameter are listed. In the second column we report the average number of lines used. Finally, in the last two columns, we show the total internal and systematic errors, derived by summing in quadrature the contributions of individual error sources.

4. Results and comparison with other studies

The first finding in the present work is that the metallicity of NGC 6388 is [Fe/H] = −0.509 ± 0.011 ± 0.024 dex (rms = 0.039 dex, 12 stars) on our metallicity scale defined by the high resolution UVES spectra (Carretta et al. 2009c). This result is strongly corroborated by the metal abundance derived from the very large sample of stars with GIRAFFE HR13 spectra: [Fe/H] = −0.488 ± 0.003 ± 0.020 dex (rms = 0.040 dex, 150 stars), where the first and second term refer to statistical and systematic errors, respectively. We plot in Fig. 4 iron abundances in NGC 6388 as a function of the effective temperatures for the present sample, to which we added the stars analysed in Carretta & Bragaglia (2018).

It should be noted that the observed star-to-star scatter in iron abundance is actually smaller than the estimate of the random errors (see previous section). Hence, the present data do not support the existence of a metal abundance spread in NGC 6388. This is the first conclusion from our homogeneous and ample data set and will be further discussed below.

Abundances from Fe II are in good agreement with results from neutral transitions. We found [Fe/H] = −0.491 dex, rms = 0.039 dex from the 12 stars with UVES spectra, and [Fe/H] = −0.478 dex, rms = 0.053 dex from 149 stars with GIRAFFE spectra. Again, the estimates of the internal errors are consistent with no significant intrinsic spread in metallicity.

Finally, we can combine the UVES sample of the present work to the sample in Carretta & Bragaglia (2018), analysed exactly with the same procedure. We obtain an average metallicity of [Fe/H] = −0.480 dex, rms = 0.045 for the total sample of 35 stars with UVES spectra, in excellent agreement with the results from GIRAFFE spectra.

In Fig. 5, we show the distribution of [Fe/H] values for our total sample of 35+150 stars in NGC 6388 as a function of the radial distance from the cluster centre. The bulk of our sample is enclosed between the half-mass radius (r_h = 0.52 arcmin, Harris 1996) and the tidal radius (r_t = 6.21 arcmin). Only six stars, members according to their RV, are found beyond this limit. However, it is not straightforward to call them extra-tidal, as the value for r_t is not univocal and may be larger. In fact, Dalessandro et al. (2008) give 7.57 arcmin (29 pc) and Baumgardt et al. (2018) have a value about three times larger (based on a tidal radius of 85.6 pc; the very large difference comes from the different methods in estimating the cluster profile, since they also use dynamical information in their modelling). We identified five of the six stars with the Vasiliev & Baumgardt (2021) catalog of membership in Galactic GCs based on *Gaia* EDR3 and only one, the closest to the centre, is considered a member. Currently, the *Gaia* astrometry has not yet reached its full potentiality, especially in crowded fields as those in GCs. On the other hand, RVs and metallicities for these five stars are indistinguishable from the bulk cluster values, hence, we considered these stars to be cluster members, with the cautionary flag that they may require further investigation. However, their membership issue does not influence the main result of our work.

We show in Fig. 6 (upper panel), the narrow [Fe/H] distribution in our sample, which displays no trend with $T_{\rm eff}$. The lower panel shows the histograms of the [Fe/H] values in our work as well as L13, M20, and H20, for comparison. We also indicate the number of stars considered in the average and the

Table 3. Atmospheric parameters and derived iron abundances in NGC 6388.

Star	$T_{\rm eff}$ (K)	log g (dex)	[A/H] (dex)	v_t (km s^{-1})	nr	[Fe/H]I (dex)	rms	nr	[Fe/H]II (dex)	rms
n63a	3772	0.80	−0.48	1.30	125	−0.476	0.214	11	−0.492	0.194
n63b	3727	0.61	−0.51	0.27	73	−0.509	0.314	5	−0.483	0.199
n63c	3714	0.58	−0.54	1.35	77	−0.552	0.220	12	−0.569	0.262
n63d	3722	0.63	−0.57	1.17	83	−0.573	0.177	18	−0.543	0.239
n63e	3820	0.93	−0.59	1.78	122	−0.494	0.151	18	−0.454	0.200
n63f	3818	0.93	−0.54	1.54	101	−0.543	0.130	14	−0.484	0.152
n63g	3708	0.52	−0.44	0.76	73	−0.436	0.216	10	−0.487	0.290
n63h	3755	0.73	−0.54	1.61	100	−0.536	0.184	14	−0.520	0.234
n63i	3793	0.85	−0.53	1.63	113	−0.528	0.142	16	−0.498	0.167
n63l	3874	1.07	−0.49	1.66	126	−0.489	0.166	15	−0.447	0.145
n63m	3777	0.80	−0.47	1.46	106	−0.468	0.186	13	−0.481	0.206
n63n	3727	0.65	−0.50	1.69	100	−0.499	0.173	10	−0.432	0.137
l63p001	4576	2.23	−0.49	1.63	21	−0.488	0.106	3	−0.524	0.077
l63p002	4712	2.40	−0.51	1.53	24	−0.513	0.121	3	−0.391	0.201
l63p003	4991	2.69	−0.41	1.82	16	−0.413	0.135	3	−0.474	0.116
l63p004	4522	2.16	−0.50	1.31	15	−0.504	0.094	3	−0.435	0.104
l63p006	4892	2.56	−0.45	2.23	19	−0.449	0.105	4	−0.468	0.119

Notes. The complete table is available at CDS, Strasbourg.

Table 4. Sensitivities of abundance ratios to variations in the atmospheric parameters and to errors in the equivalent widths, and errors in abundances for stars of NGC 6388 observed with UVES.

Element	Average n. lines	$T_{\rm eff}$ (K)	log g (dex)	[A/H] (dex)	v_t km s^{-1}	EWs (dex)	Total internal	Total systematic
Variation		50	0.20	0.10	0.10			
Internal		6	0.04	0.04	0.12	0.02		
Systematic		17	0.06	0.02	0.04			
[Fe/H]I	100	−0.027	+0.041	+0.023	−0.044	0.016	0.058	0.024
[Fe/H]II	13	−0.119	+0.122	+0.040	−0.030	0.045	0.072	0.055

Table 5. Sensitivities of abundance ratios to variations in the atmospheric parameters and to errors in the equivalent widths, and errors in abundances for stars of NGC 6388 observed with GIRAFFE.

Element	Average n. lines	$T_{\rm eff}$ (K)	log g (dex)	[A/H] (dex)	v_t km s^{-1}	EWs (dex)	Total internal	Total systematic
Variation		50	0.20	0.10	0.10			
Internal		6	0.04	0.04	0.22	0.03		
Systematic		57	0.06	0.02	0.01			
[Fe/H]I	20	+0.014	+0.032	+0.022	−0.060	0.027	0.067	0.020
[Fe/H]II	3	−0.079	+0.118	+0.040	−0.018	0.070	0.079	0.097

rms scatter obtained in each analysis. The information is summarised in Table 6 where we report also the type of spectra used in each analysis and their spectral resolution. Further details are discussed in the following subsections.

Mean [Fe/H] values and associated rms scatters from the present work and from literature studies are plotted for NGC 6388 in Fig. 7. For the present work, we distinguish the metallicity obtained from UVES (right blue point) and GIRAFFE (left red point) spectra. For the analysis by M20, the [Fe/H] value and the scatter on the right are from the selected sample of stars with $S/N > 70$ (see below). For H20, the rightward value is the one derived from their HB method (see below).

4.1. Comparison with L13

Lanzoni et al. (2013) were mostly concerned with the kinematics of the cluster, for which they acquired SINFONI low resolution, near-IR spectra in the innermost part and FLAMES spectra (GIRAFFE setup HR21, plus UVES 580) in the external regions, adding also FLAMES archive data. However, to better cull out non-member stars, they also derived metallicities for a limited number of giants in their sample. The classical abundance analysis with EWs was used for spectra available in the ESO archive at the epoch (UVES and GIRAFFE HR11, HR13), whereas for the larger number of stars with HR21 spectra, metal abundances were obtained from a calibration of the CaT method.

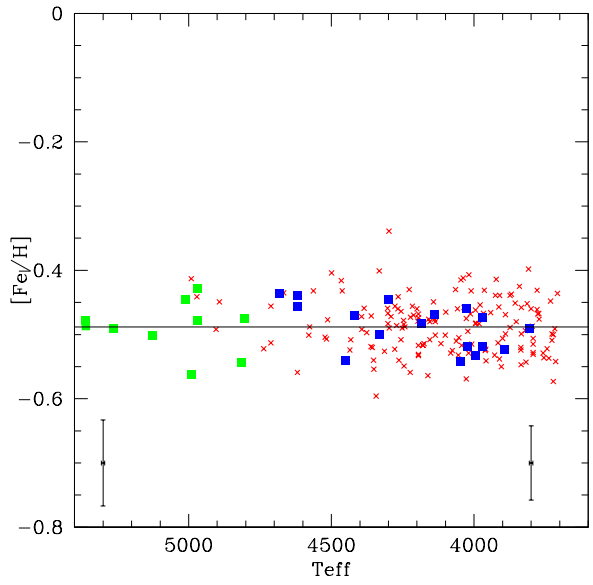

Fig. 4. Iron abundances in NGC 6388 as a function of effective temperature from the present work and Carretta & Bragaglia (2018). Symbols for the evolutionary stages are as in Fig. 1. Error bars on the left and on the right are internal errors for abundances derived from GIRAFFE and UVES spectra, respectively.

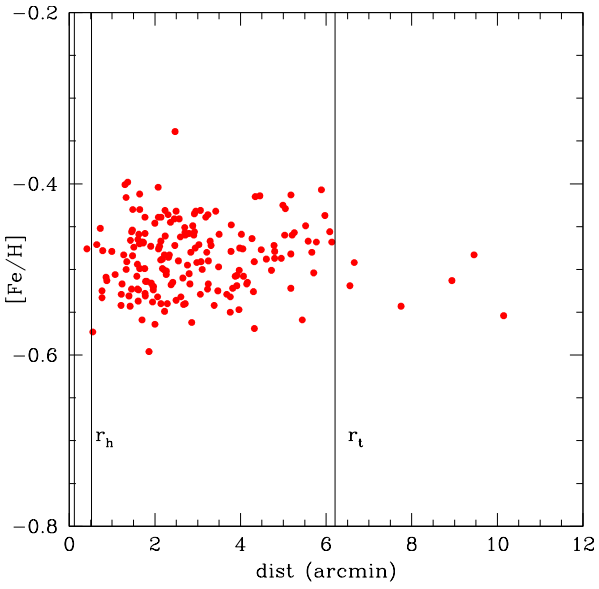

Fig. 5. Distribution of [Fe/H] ratios for our total sample (35 UVES and 150 GIRAFFE) as a function of the distance from the cluster center. The solid lines are traced at the core radius, the half-mass radius, and the tidal radius from Harris (1996).

The average value of [Fe/H] from 276 stars is = −0.401 dex, with σ = 0.078 dex. Unfortunately, not many details nor an error budget were provided concerning the abundance analysis, so that a formal conclusion about the metallicity spread is not possible. However, we note that L13 did not claim that an intrinsic spread was present in NGC 6388.

In Fig. 8 we plot the difference in [Fe/H] (in the sense L13-us) as a function of effective temperature for 151 stars present in both studies. The mean difference is 0.098 dex, with an rms scatter of 0.086 dex. Although it is scarcely significant, this offset can be ascribed to a number of reasons, including a difference in the solar reference abundance, not provided in L13.

Table 6. Information on metallicity of different data sets.

Sample	[Fe/H]	rms	Nr	Resol	Note
us	−0.488	0.040	150	26400	GIRAFFE HR13
	−0.480	0.045	35	47000	UVES
L13	−0.401	0.078	276	18000	GIRAFFE HR13,HR21
M20	−0.407	0.164	24	22500	APOGEE,all stars
	−0.436	0.077	9		APOGEE, $S/N > 70$
H20	−0.43	0.48	4098	2800	MUSE; their tab.7
	−0.52	0.27	741		HB method, see text

However, we were able to identify 43 stars that were analysed by L13 using methods similar to those we adopted in our study, with temperature and gravity data from photometry and EWs measured on high or intermediate-resolution UVES and GIRAFFE HR11 and HR13 spectra. Those are stars for which spectra were in the ESO archive in 2013, essentially those analysed in Carretta et al. (2007a, 2009b) along with a few stars from the program by Catelan, recently studied by Carretta & Bragaglia (2018). We indicate them with blue symbols in Fig. 8 and we can immediately see that the set of these stars defines a sequence with a lower scatter with respect to the whole sample, apart from three outliers. We found an average difference in [Fe/H] = 0.064 dex (L13-us), with σ = 0.053 dex from 40 stars, which have a mean metallicity of −0.412 dex in L13, with σ = 0.059 dex. This scatter is in good agreement with our findings, it leaves no space for an intrinsic spread in metal abundance, and it suggests that large part of the difference and scatter shown in Fig. 8 has to be ascribed to stars whose metallicity was obtained from HR21 GIRAFFE spectra using the CaT method.

4.2. Comparison with M20

Mészáros et al. (2020) published results based on APOGEE DR16 for 31 GCs; for NGC 6388 there are 24 stars observed, but only 9 stars (of which 7 in common with ours) pass their suggested quality cuts, namely, $S/N > 70$ and $T_{\rm eff} < 5500$ K. Average values for them are given in Table 6. In particular, for the high-quality sample, the average value is [Fe/H] = −0.436 dex with a spread of 0.077 dex, to be compared to an internal error of 0.152 dex (M20). Again, no indication of iron spread is present. We recall that M20 detected a significant iron spread only for ω Cen; they did not find metallicity variations for any of the iron-complex GCs (type-II GCs) in their sample, namely, NGC 362, NGC 7089, NGC 6388 and, notably, NGC 1851 and M 22 (NGC 6656).

For NGC 6388, we found 22 stars in common between the present work and M20. The difference in [Fe/H] (in the sense M20 – us) is plotted in Fig. 9 as a function of the effective temperature. The average difference is 0.092 dex (σ = 0.178 dex, 22 stars). On the other hand, if we consider only stars that pass the quality criteria recommended by M20 (indicated by blue symbols in Fig. 9), the difference is almost unaltered (0.072 dex), but the dispersion is more than halved (σ = 0.082 dex, 7 stars). This comparison suggests that using lower S/N spectra may result into an artificially larger spread, despite using the same method of abundance analysis. The average metallicity derived from the seven stars in common, with $S/N > 70$ spectra in APOGEE, is [Fe/H] = −0.427 dex. Taking into account the −0.09 dex offset due to different solar reference abundances, the value corresponds to [Fe/H] = −0.517 dex on our abundance scale, which is

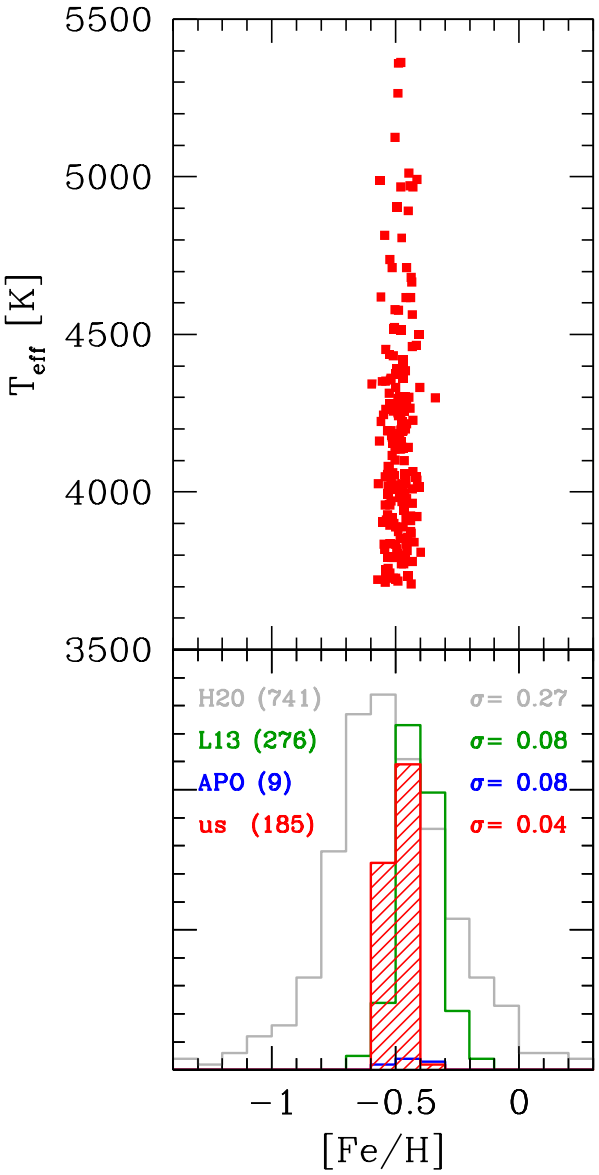

Fig. 6. Distribution of metallicity of NGC 6388 stars. *Upper panel*: distribution of our [Fe/H] values in NGC 6388 as a function of $T_{\rm eff}$. *Lower panel*: histogram of metallicity in the various studies considered: this work (red shaded histogram), L13 (green), M20 (APOGEE, blue), and H20 (grey). For each sample the number of stars and the rms scatter are also listed (see also Table 6).

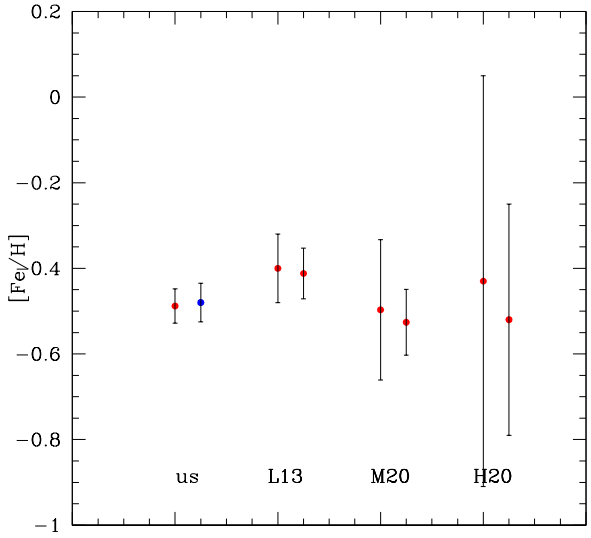

Fig. 7. Average metallicity and associated rms scatter for NGC 6388 resulting from the present work (the blue circle on the right indicates the value from UVES spectra, the red one is for GIRAFFE spectra) and from literature studies. The rightward point for L13 refers to the analysis made with EWs (and not with the CaT). The rightward point for M20 refers to the value obtained considering only the high S/N spectra and the rightward point for H20 is derived from their HB method (see text).

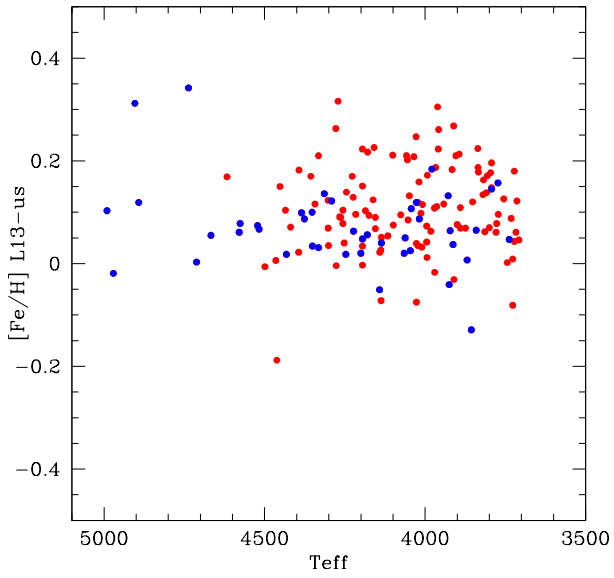

Fig. 8. Difference in metallicity between the present work and L13 as a function of the effective temperature. Blue circles indicate stars whose analysis in L13 was based on EW measurement on UVES and GIRAFFE HR11, HR13 spectra. Red points refer to stars analysed with the CaT method from GIRAFFE HR21 spectra in L13.

in excellent agreement with the results obtained in the present work. The points for M20 in Fig. 7 were also shifted to our scale of solar abundance by using the above offset.

4.3. Comparison with H20

The case of H20 is complex, as those authors found a complex structure in the metallicity distribution and a large dispersion (even larger than for ω Cen, before taking into account the errors, see below). They employed MUSE on RGB stars in 25 MW GCs, among which NGC 6388, to derive their metallicity. The low-resolution MUSE spectra were acquired in the central parts, namely, the same covered by the HST UV Survey (see below) and were used to derive metallicity through the CaT method. This technique requires a calculation of W', the so-called reduced EWs, which are then used to calibrate a relation with metallicity, using literature reference values. Husser et al. (2020) used four different methods to calculate W', which they indicated as 'HB' (using only stars brighter than V(HB)+0.2 and a linear relation with V-V(HB); this is generally used in literature), 'all' (using all RGB stars and a quadratic relation with V-V(HB)), 'M' (same as 'all', but using the absolute magnitude in the F606W band), and 'lum' (same as previous ones, but using the luminosity). We refer to H20 for more details.

For NGC 6388, H20 cite an average value [Fe/H] = −0.43 (σ = 0.48) dex for the whole cluster (4098

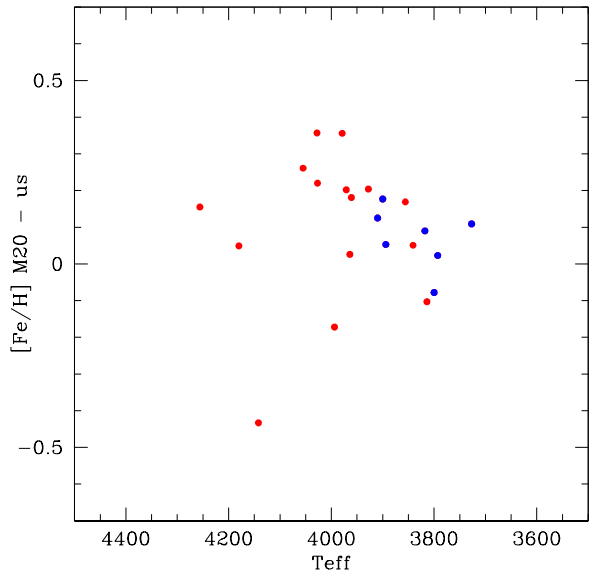

Fig. 9. Difference in metallicity between the present work and M20 as a function of the effective temperature for stars in common between the two studies. Blue circles indicate stars which pass in APOGEE the quality cuts recommended by M20, namely $S/N > 70$ and $T_{\rm eff} < 5500$ K.

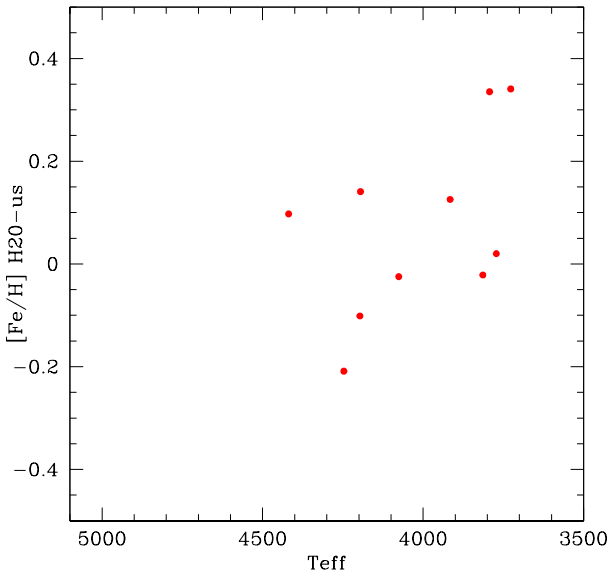

Fig. 10. Difference in metallicity between the present work and H20 as a function of the effective temperature for stars in common. For H20, metallicities obtained with the HB method were adopted.

stars) and we calculated −0.52(σ = 0.27 dex) for the 741 stars for which W' is calculated with the HB method. As they were studying the GCs in the multiple populations scenario, they also calculated the metallicity separately for what they indicate as population P1, P2 (P and I+E in the Carretta et al. 2009b division) and P3, which is the 'anomalous' component, on the red RGB (see Milone et al. 2017 and below). The values for mean [Fe/H] and σ are −0.45, 0.45 dex for 579 P1 stars, −0.44, 0.42 dex for 1203 P2 stars, and −0.25, 0.39 dex for 411 P3 stars (we note that these numbers can be summed up to 2193, i.e., not all the sample was assigned to a given component). We caution, however, that the fraction of the P3 component in H20 (411/2193=0.187) is quite different from the estimate by Milone et al. (2017) for NGC 6388 (0.299). Husser et al. also claim to find indications of metallicity variations among P1 stars for NGC 6388 and the other type-II GCs observed, but they do not consider it definitively proven.

The large dispersion and the difference in metallicity between P1,P2, and P3 are taken with caution by H20, who comment that the errors are large for NGC 6388 and its so-called twin NGC 6441, due to a combination of crowding affecting the photometry, differential reddening, and high metallicity. For comparison, ω Cen, with a well documented wide metallicity dispersion and a much clearer structure and separation both in the CMDs and in the chromosome map (see next section), has a similar dispersion, but with a smaller associated error. From Fig. 17 in H20, the uncertainty in [Fe/H] has a peak value of more than 0.15 dex and a very broad, asymmetric distribution for NGC 6388, compared to about 0.10 dex or less, along with a more peaked distribution for most of the other GCs. In fact, once the uncertainties have been taken into account, the intrinsic metallicity distribution for ω Cen has a σ of about 0.4 dex (from their Fig. 18); while for NGC 6388, we read a value slightly more than 0.2 dex. A real spread appears to be present, according to H20, which is at odds with the findings of other studies. However, we note that due to the problematic photometry of this heavily contaminated bulge cluster, which affects spectra extraction from MUSE data cubes, Pfeffer et al. (2021) concluded that NGC 6388 has no spread in iron.

Since the MUSE observations cover only the very central part of the cluster, the intersection with our FLAMES data is small. We found only 11 stars in common (10, considering the HB method) and we compared the metallicity results in Fig. 10. Since H20 only published EWs and corresponding metallicities, we used our values of $T_{\rm eff}$ in the figure, as in previous comparisons with L13 and M20. The mean difference in metallicity between our values and H20 is 0.070 dex (in the sense H20 minus us), with σ = 0.176, but a clear trend is visible in the figure. At higher temperatures, the metallicities from H20 are lower than ours, whereas at lower temperatures, they find higher metal abundances with respect to our values. Given the small number of stars in common, we cannot pursue the comparison further and draw firm conclusions.

Finally, if we compare Fig. 20 in H20 with Fig. 27 in Marino et al. (2019), we note a possible discrepancy in the arrow describing the effect of a change in metallicity of 0.15 dex in the position in the ChM. In both cases an increase in metallicity produces an increase in the $\Delta_{\rm F275,F814}$ pseudocolour, but while in the first case the arrow is directed upward, in the second it is almost orthogonal and directed downward.

4.4. No metallicity spread in NGC 6388

The comparisons in the above sections point out the risks related to using low resolution or low S/N spectra. In particular when dealing with metal-rich stars, there is the danger to introduce a spuriously enhanced spread which is not an intrinsic feature, but in part an artefact of the analysis.

On the other hand, the dispersion associated to the [Fe/H] values from our present analysis, based on high resolution spectra, excludes the existence of a noticeable intrinsic metallicity spread in the large sample of analysed stars in NGC 6388, when coupled to the estimate of internal errors. Two further tests were performed to confirm this result.

First, we used the algorithm illustrated by Mucciarelli et al. (2012, kindly made available to us) to estimate the mean and

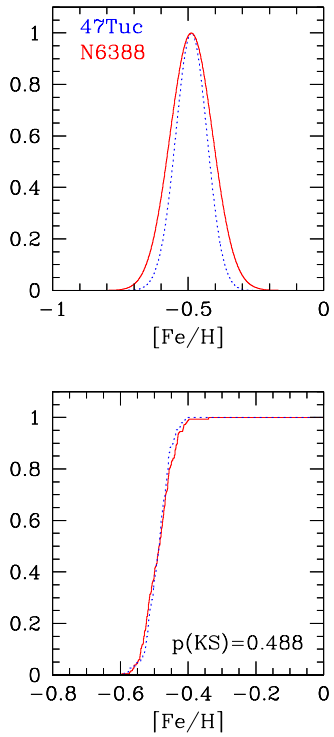

Fig. 11. Comparison of the metallicity distributions in NGC 6388 and 47 Tuc. *Upper panel*: generalised histogram of [Fe/H] values for NGC 6388 (red solid line) and 47 Tuc (blue dotted line, from Carretta et al. 2009a,b), normalised to their maximum. *Lower panel*: two-tail Kolmogorov-Smirnov test for the above metallicity distributions. The K-S probability is also listed.

intrinsic spread of an elemental ratio ([Fe/H] in our case) by maximising the likelihood function defined as in their Sect. 2.1. For NGC 6388 we obtained an average value of −0.484 dex and a zero intrinsic dispersion for the metallicity of the 185 stars in our sample ($\sigma_{\rm intr}$ = 0.000 ± 0.008).

Furthermore, we compare the generalised histograms for NGC 6388 from the present work and for 47 Tuc from Carretta et al. (2009a,b) in Fig. 11 (upper panel). The GC 47 Tuc was selected because it is analysed exactly in the same way as NGC 6388, its sample is almost as large (147 stars) as the present sample, and it is the most metal-rich GC in our homogeneous FLAMES survey, beside NGC 6388. Last but not least, 47 Tuc is one of the best representative of the class of monometallic GCs, never suspected to host a metallicity dispersion (see Carretta et al. 2004, 2009a,b; Cordero et al. 2014). The sigma of the gaussian centered at each data point used to generalise the histogram was chosen equal to the error on each point, namely 0.067 dex for NGC 6388 (from Table 5) and 0.047 dex for 47 Tuc (from Carretta et al. 2009b). These values correspond to the internal errors derived for stars with GIRAFFE spectra, representing the vast majority in the samples.

After applying an offset of 0.255 dex to account for the difference in the mean metallicity of the two GCs, the histograms are superimposed in the upper panel of Fig. 11. The metallicity distribution for each cluster is well described by a single symmetric Gaussian curve. This comparison reveals only a negligible difference in the spread, that can be fully ascribed to the different internal errors associated to the analyses. A two-tail Kolmogorov-Smirnov test (lower panel of Fig. 11) clearly indicates that the null hypothesis (the two distribution are extracted from the same parent population) cannot be rejected.

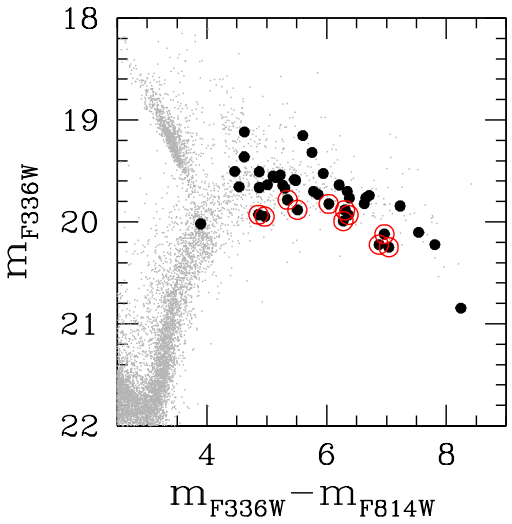

Fig. 12. $m_{\rm F336W} - m_{\rm F814W}$ versus$m_{\rm F336W}$ for NGC 6388 (selecting only stars with a valid sharpness parameter (for details, see text)). Stars in our spectroscopic sample are indicated by larger black dots, while stars selected on the redder part of the RGB are shown as red circles.

Our analysis, the above tests, and the comparison with other literature data (see above) allow to conclude that in NGC 6388 there is no evidence for an intrinsic metallicity dispersion. This is an important piece of information for a type-II GC.

5. Discussion

The so called 'anomalous' RGB stars should be subjected to further investigation to clarify their nature and role in defining a separate class of GCs. In the next subsections, we associate the metallicities we obtain from our large sample to the UV HST photometry and we discuss the properties of so-called type-II GCs.

5.1. Chromosome map and metallicity

Neither Piotto et al. (2015) nor Milone et al. (2017) published a classification of individual stars in their full GC sample into FG, SG, and red-RGB stars. These data only exist for six GCs out of 58 objects and, unfortunately, NGC 6388 (or any other type-II GC) is not among them.

We then downloaded the available HUGS catalogue (Nardiello et al. 2018a)[3], who published the photometry uncorrected for reddening and without distinction between stars of different populations. Starting from these data we followed the necessary steps to produce the pseudo-colours maps used in that survey to single out different populations in GCs. However, we did not apply corrections for differential reddening, which is outside the goal of the present study and which is not indispensable for establishing the lack of any metallicity variation among stellar populations in NGC 6388.

From the CMD shown in Fig. 12 we identified stars in common between our spectroscopic sample and the HST photometry by Nardiello et al. (2018a). A few stars along the redder part of the RGB have been highlighted (red circles) in the plot to reproduce Fig. 16 in Milone et al. (2017). These red-RGB stars also show up in a given region of the ChM only in type-II GCs.

[3] https://archive.stsci.edu/prepds/hugs/

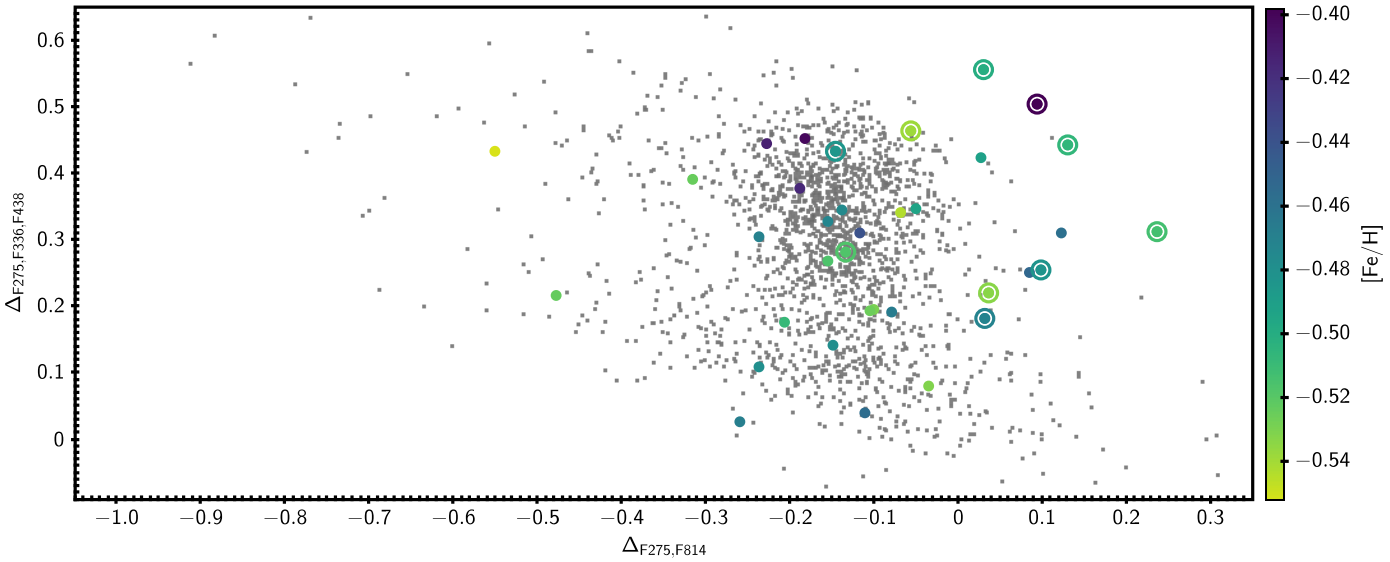

Fig. 13. Position of the stars in NGC 6388 in the so-called ChM map (Milone et al. 2017). Stars also in our spectroscopic sample are showed as large filled circles, coloured with their metallicity. Stars selected on the red part of the RGB (see text and previous figure) are indicated by large open circles.

Following the discussion in Nardiello et al. (2018a), we kept only stars with good quality photometry. In particular. we excluded stars with the 'sharpness' parameters outside the ±0.15 range in any of the filters; no cut on the error was applied, as all the stars involved in the ChM are giants and the corresponding errors are very small and uniform. As in Milone et al. (2017) we used stars in the magnitude range m_{F814W} = 14−18, computed the colours and pseudo-colours $col_1 = (m_{F275W} - m_{F814W})$ and $col_2 = (m_{F275W} - 2 \times m_{F336W} + m_{F438W})$, and defined lines describing the limits of the RGB stars in the corresponding plots. Finally, we computed the values for $\Delta_{275,814}$ and $\Delta_{275,336,438}$ from Eqs. (1) and (2) in Milone et al. and using the RGB widths in their Table 2.

The resulting two-pseudocolours diagram is shown in Fig. 13, which reproduces sufficiently well the plot in Fig. 3 of Milone et al. (2017) and the location of the different populations: FG stars, SG stars, and the region where the 'anomalous' red-RGB stars are arranged in this diagram. Further refinement is beyond the main goal of the paper and we await the publication of the ChM by the group, who have produced them homogeneously, for further discussion.

In Fig. 13, we identify the few stars selected on the redder RGB with concentric open circles. Milone et al. (2017) claim that all evidence supports that stars in the red-RGB are enhanced in C+N+O, in s-process elements, and in iron. This is, for instance, true for NGC 1851, where we detected both a small iron spread and an enhancement in *s*-process elements on the red-RGB we defined using Strömgren filters (Carretta et al. 2010b, 2011; see also below). However, we do not find a significant spread in Fe in NGC 6388 and, in particular, we do not find a metallicity enhancement for the red-RGB stars (see Fig. 13). We stress that this conclusion is not strictly related to our method of reproducing the ChM, which shows resemblance, both to the one in M17 and to that recomputed by H20. Milone et al. (2017) list a fraction 0.299 ± 0.016 of type-II stars with respect to the total number of analysed stars in NGC 6388, while H20 have a lower value. A third (or about one fifth, as in H20) of stars with enhanced metal abundance would have been easily discerned in the distribution of [Fe/H] values (considering that we observed stars also on the red-RGB), resulting in a clearly detectable iron spread. From our data, this is not the case.

Table 7. Fraction of stars in type-II GCs from H20 and M17.

GC	Fraction H20	Fraction M17
362	0.027 ± 0.006	0.075 ± 0.009
1851	0.330 ± 0.020	0.300 ± 0.014 [(a)]
5139	0.518 ± 0.023	0.640 ± 0.018
5286	0.157 ± 0.015	0.167 ± 0.010
6388	0.187 ± 0.009	0.299 ± 0.016
6656	0.479 ± 0.033	0.403 ± 0.021
7078	0.331 ± 0.019	0.050 ± 0.010 [(b)]
7089	0.025 ± 0.005	0.043 ± 0.006

Notes. [(a)]From Gratton et al. (2019). [(b)]From Nardiello et al. (2018b).

5.2. Characterising a type-II cluster

With the present large sample of stars analysed spectroscopically, we can add NGC 6388 as a good test for comparing spectroscopy and UV photometry concerning the classification of GCs. When discussing the type-II GCs as a separate class, we must first note that the fraction of 'peculiar' stars deduced from the ChM and photometric methods exhibit some degree of subjectivity; as evident from Table 7 and Fig. 14, where we compare the fraction of the so called type-II stars for eight GCs analysed by two groups starting from the same HST photometry. Values of the fractions and associated errors for M17 are taken from their Table 2 (for NGC 1851 we use the fraction corrected for a misprint as in Gratton et al. 2019, their Table 5). To those, we added the corresponding value for NGC 7078 (M 15) from Nardiello et al. (2018b) who considered also this GC as a type-II cluster from the analysis of its pseudo-colour diagrams. For H20, we computed the ratios using the fraction of their P3 stars over the total of P1+P2+P3 populations from their Table 7. For the very complex cluster ω Cen, we adopted as type-II stars the sum

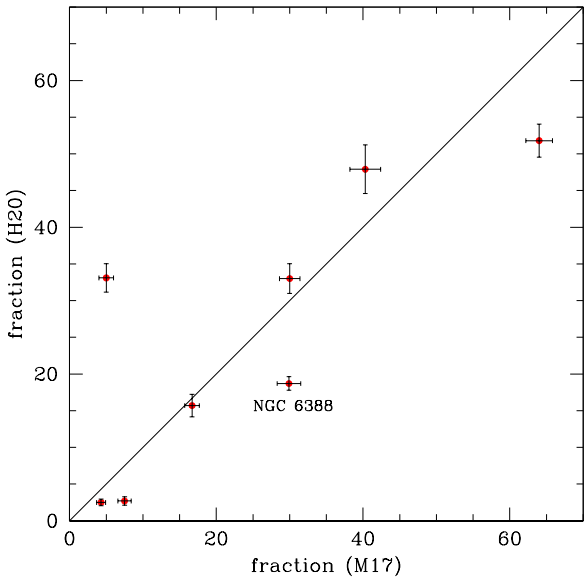

Fig. 14. Comparison of fractions of type-II stars in 8 GCs in common between the studies by H20 and M17 (plus Nardiello et al. 2018b for NGC 7078/M 15). The line of equality is also shown and the position of NGC 6388 is labeled in the plot.

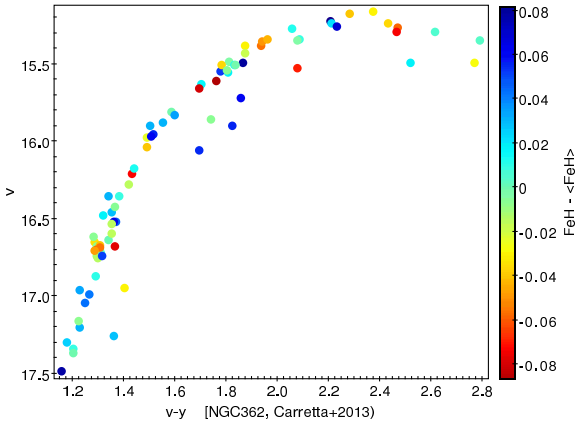

Fig. 15. Strömgren CMD $v - y$ vs. v from Carretta et al. (2013). Stars are coloured with a palette indicating the deviations from the average metallicity of the cluster.

of the populations from P4 to P9, as a visual comparison with M17 showed that the normal stars are only restricted to population P1+P2+P3. The error bars are assumed from the Poisson statistics.

Figure 14 shows that the estimates of the fractions are more or less distributed around the equality line, but in a few cases the values can be very different, although the underlying photometric database is the same. The only GC for which there is a formal agreement within one Poisson error bar is NGC 5286. In other cases, such as NGC 362, NGC 1851, and ω Cen, the discrepancies are not large. On the other hand, NGC 7078 (M 15) and NGC 6388 have the largest differences in the estimated fractions. This indicates that a more objective criterion to separate the so called type-II stars is required.

Milone et al. (2017) state that a type-II GC is identified by (at least) one of the following properties: split SGB even in optical photometric bands, multiple sequences in the ChM, and wide range in heavy elements, including iron and extending to the species produced by *s*-process. The sample of so called type-II GCs seems to be, however, a heterogeneous class. This motley group contains the two most massive GCs of our Galaxy, that most probably were the nuclear star clusters of past dwarf galaxies later incorporated in the Milky Way, namely NGC 5139 (ω Cen) and NGC 6715 (M 54, see e.g., Bekki & Freeman 2003; Bellazzini et al. 2008; Carretta et al. 2010c; see also Massari et al. 2019 who associate the first to *Gaia*-Enceladus and confirm the association with Sagittarius of the second, using *Gaia* data). Both GCs probably experienced multiple bursts of star formation over their entire life (see e.g., Johnson & Pilachowski 2010; Siegel et al. 2007). In both cases, the metal-rich component according to the spectroscopy represents a fraction of the total mass roughly in agreement with the estimated fraction of type-II stars from photometry, with evidence of enhancement also in *s*-process elements.

However, to the same group also belong two smaller GCs, less luminous by two orders of magnitude: NGC 1261 and NGC 6934. Small spreads in [Fe/H] (0.1–0.2 dex) were detected for these lower mass GCs attributed to the type-II class (Muñoz et al. 2021; Marino et al. 2021 for NGC 1261 and Marino et al. 2021 for NGC 6934). These results are based on samples of limited size, much smaller than for the GCs discussed above. Marino et al. (2021) also note that for both clusters no enhancement in *s*-process elements is found and suggest this is due to the low mass of these GCs. A comparison of the fractions determined by photometry and spectroscopy would be meaningless, since only 8–14 stars in NGC 1261 and 13 stars in NGC 6934 were observed with high-resolution spectroscopy.

Coming to the intermediate-mass GCs, the existence of a secondary, redder RGB sequence in a few GCs (besides ω Cen) is known since more than one decade (it was discovered in NGC 1851 by Han et al. (2009) for the first time, using the *U* and *I* filters). Carretta et al. (2011, 2013) discussed the cases for NGC 1851 and NGC 362 using Strömgren photometry and their own spectroscopic results. In NGC 362 Carretta et al. (2013) discovered that in the Strömgren $v - y$ colour the RGB is clearly split, with a minority of stars (~6%) defining a secondary, redder sequence only populated by Ba-rich stars (roughly corresponding in size to the type-II component claimed from UV photometry in M17). The same phenomenon was also traced by Carretta et al. (2011) in NGC 1851, where the redder $v-y$ colour was attributed most likely to large enhancement in N (see also Carretta et al. 2014 and Villanova et al. 2010).

Both GCs are now classified as type-II clusters. However, in NGC 362 no spread in [Fe/H] was detected above the small level (0.041 dex) fully explained by internal uncertainties in the abundance analysis. This is shown in Fig. 15, where the CMD of NGC 362 in Strömgren photometry is coloured based on the difference in iron with respect to the average [Fe/H] value in this GC. However, the trickling of stars in this red sequence does not present any enhanced [Fe/H] distribution with respect to the other giant stars.

In NGC 1851, instead, a small metallicity dispersion was found; however, the best results were obtained from a cluster analysis using a *k*-mean algorithm and the run of [Fe/H] as a function of [Ba/H] as representative of the *s*-process elements (Carretta et al. 2011). With this technique, two stellar component were unveiled, the most metal-rich being also more rich in Ba and *s*-process elements, with Strömgren photometric indices consistent with an overabundance in carbon. The fraction of this component from spectroscopy is roughly compatible with the fraction of type-II stars from the HST photometry, both from M17 and H20.

The largest fraction of type-II stars, excluding ω Cen and M 54, belongs to NGC 6656 (M 22), which has an iron spread of about 0.14 dex according to Marino et al. (2011), besides all other characteristics of type-II clustes. As a caveat, the metallicity spread has been questioned by Mucciarelli et al. (2015) who attributed the result to the adoption of surface gravities derived from spectroscopy. Those values correspond to unrealistic low stellar masses, whereas using photometric $\log g$ values no evidence of spread was found from singly ionised iron, at variance with Fe I. Mucciarelli et al. concluded that this pattern could be explained by non-LTE effects, namely overionisation, lowering abundances from Fe I while leaving unaltered those from Fe II. The surface gravity values used in our present analysis for NGC 6388 (the fourth in line for type-II stars fraction, according to M17) were derived from the photometry and we did not find evidence of different iron abundances in the large fraction of stars dubbed as type-II, as discussed above.

To conclude, in a fraction of GCs classified as type-II no metallicity spread is detected over large sample of stars. Some GCs show an enhancement in *s*-process elements but not in iron (e.g., NGC 362). In other cases, such as NGC 1261 and NGC 6934, the contrary is observed. Finally, for M 15 the large dispersion measured for neutron-capture elements is known to be originated by the *r*-process (e.g., Sneden et al. 2000; Sobeck et al. 2011; Worley et al. 2013; Kirby et al. 2020) and not by the *s*-process, as found for some other type-II GCs. Models of fast-rotating massive stars (also called 'spinstar', Frischknecht et al. 2016; Limongi & Chieffi 2018) would show an increase of *s*-process yields, but would provide also alterations in light-elements, which are not seen to be correlated to abundance variations in neutron-capture elements in M 15 or other GCs (e.g., Roederer 2011). Moreover, no evidence of a spread in iron is claimed on the basis of extant high-resolution spectroscopy (e.g., Carretta et al. 2009a,b).

All the above considerations were based on the metallicity spreads (or their absence) derived in the original studies. For a more homogeneous approach, we evaluated the iron dispersion of each type-II GC using the same method (see Sect. 4.4) we employed for NGC 6388, namely, a maximisation of the likelihood function as defined by Mucciarelli et al. (2012), which estimates the intrinsic spread by taking into account also the errors. In addition to the GCs listed as type-II in M17 and Nardiello et al. (2018b), we also added NGC 6273, as done in Gratton et al. (2019). This GC was not classified by M17 as a type-II because it lacks the UV HST photometry, however it clearly shows a large iron variation among its stellar populations (Johnson et al. 2015, 2017). Results are given in Table 8, where we list the adopted internal error for the metallicities of the individual stars, the derived intrinsic spread and the associated uncertainty, the number of stars, and the reference for the abundance analysis. To stay on the safe side, we conservatively chose to use the internal errors derived for stars with GIRAFFE spectra (usually larger than those for stars with UVES spectra) for NGC 6388 and the other GCs from our group (NGC 362, NGC 1851, NGC 6715, and NGC 7078).

From this table we see that the procedure confirms the zero intrinsic metallicity spread for NGC 362 and the large iron spreads in NGC 5139, NGC 6273, NGC 6715, and NGC 7089. Smaller but robust spreads are derived in NGC 5286 and NGC 6934. A few GCs merit further comments. The case of NGC 1851 was already discussed above: the best separation of populations requires both [Fe/H] and the [Ba/H] abundances, but a small spread is still confirmed by iron abundances only.

Table 8. Intrinsic spreads in iron.

NGC	Error	$\sigma_{\rm intr}$	err_σ	Stars	Refs.
362	0.041	0.000	0.014	92	Carretta et al. (2013)
1261	0.060	0.098	0.034	8	Muñoz et al. (2021)
	0.090	0.000	0.030	14	Marino et al. (2021)
1851	0.043	0.026	0.006	124	Carretta et al. (2011)
5139	0.117	0.247	0.007	855	Johnson & Pilachowski (2010)
5286	0.075	0.078	0.013	62	Marino et al. (2015)
6273	0.026	0.181	0.018	51	Johnson et al. (2017)
6388	0.067	0.000	0.008	185	This paper
6656	0.100	0.000	0.112	35	Marino et al. (2011)
6715	0.026	0.184	0.015	76	Carretta et al. (2010d)
6934	0.090	0.089	0.035	13	Marino et al. (2021)
7078	0.040	0.042	0.008	52	Carretta et al. (2009a,b)
7089	0.072	0.268	0.054	14	Yong et al. (2014)

The case of NGC 1261 is more uncertain. For this GC, two studies, both resting on small samples, give different results, although in both the original papers the quoted spread is the same (about 0.1 dex). The cause is probably related to the smaller internal error estimated in Muñoz et al. (2021), whereas the one in Marino et al. (0.09 dex) is almost the same of the observed iron spread.

The null spread for NGC 6656 is, prima facie, unexpected. M 22 seems to be a genuine type-II GC, showing all the required features; however, the rather large internal error from Marino et al. (2011), which we derived from an average of all values associated to spectra from different telescopes, may reconcile the present finding with the usually assumed value of about 0.15 dex spread in the cluster. Finally, with this method, also NGC 7078 seems to have a (small) intrinsic iron spread, contrarily to what derived from a simple comparison of observed spread and internal errors in the analysis. However, M 15 is the most metal-poor GC in our FLAMES survey, and the analysis of GIRAFFE spectra was rather difficult. Conservatively, for the value derived in Table 8 we retained only stars with at least six measured Fe lines. This cluster surely merits further attention and a larger data set of good quality spectra. A forthcoming paper on a new abundance analysis in M 15 is in preparation.

The intrinsic iron spread does not show a significant correlation with the GC present-day masses (as represented by the model-independent total absolute luminosity M_V), as shown in the left panel of Fig. 16. The probability associated to the Pearson linear regression coefficient is only $p = 0.119$. We thus confirm the findings by Muñoz et al. (2021), who found no trend with the mass, although using a more heterogeneous set of observed spreads. In Fig. 16, a solid line connects the two different values derived for NGC 1261, but all the regressions are computed using the non-null spread for this GC from Muñoz et al. (2021). A marginally significant ($p = 0.045$) trend is observed as a function of the initial total cluster mass (central panel of Fig. 16, as estimated by Baumgardt et al. 2018). This correlation is probably due to the fraction of SN ejecta retained in type-II GCs being a function of the (original) cluster mass, as discussed, for instance, by Renzini et al. (2015) and Gratton et al. (2019).

Finally, in the right panel of Fig. 16 we plot a relation with a high level of significance ($p = 0.012$) showing that the intrinsic spread is well correlated to IQR[O/Na], the interquartile range of the [O/Na] abundance ratio, from Carretta (2019). This quantity is a measure of the extent of the Na-O anti-correlation. It may seem odd to see this quantity connected to the iron spread in GCs, as none of the early producers of the alterations in light

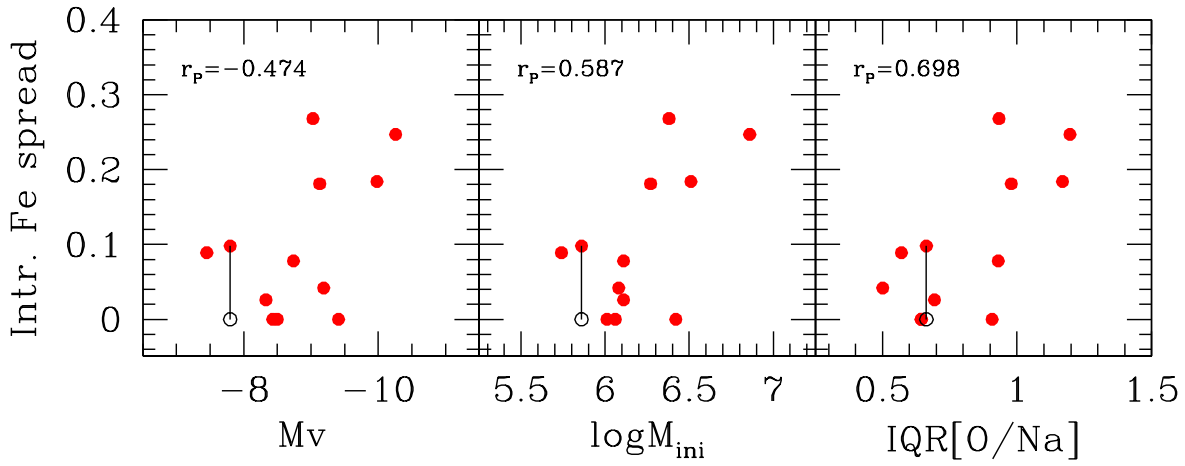

Fig. 16. Intrinsic spread in iron as a function of the total cluster absolute magnitude M_v (from Harris 1996, 2010 edition), logarithm of the initial mass (from Baumgardt et al. 2018), and IQR[O/Na] (from Carretta 2019), from left to right. In each panel we indicate the Pearson coefficient r_P (see text for the significance level). A line connects the two values for NGC 1261 from different studies.

elements are predicted to pollute the cluster environment with additional iron. However, we recall that each of the involved quantities is a strong function of the GC total mass (see e.g., Carretta 2006, 2019, M17) and this occurrence explains the above correlation well.

To conclude this discussion, the evidence suggests that either the group of GCs called type-II is heterogeneous or NGC 6388 is not a genuine type-II GC. Together with the previous analysis, the present results for NGC 6388 would require us to explain the origin of the red-RGB sequence and their position in the ChM, as well as the discrepant fractions found for some GCs by different groups, which lays claim to a less subjective definition or more published data.

6. Summary

We present a large sample of homogeneous metallicities derived for giant stars in the massive bulge GC NGC 6388. We combined new observations with archival data and previously published data obtained with intermediate and high-resolution spectroscopy for a total of 150 stars with spectra from GIRAFFE (high resolution HR13 setup) and 35 stars with spectra from UVES/FLAMES at the ESO-VLT UT2 telescope. The radial velocities, atmospheric parameters, and resulting abundances of [Fe/H] were homogeneously obtained with the same methodology and on the same scale used for the other GCs in our FLAMES survey (e.g., Carretta et al. 2006, 2010a).

The most important result we found is that NGC 6388 does not show any intrinsic metallicity dispersion. This is at odds with what found by H20 using low-resolution MUSE spectra. The rms values obtained from the 35 stars with UVES spectra and 150 stars with GIRAFFE spectra are 0.045 dex and 0.040 dex, respectively, fully compatible with the uncertainties of the analysis. Our result confirms the absence of a significant metallicity spread found by all other previous works based on spectra with sufficiently high resolution and S/N: Carretta et al. (2007a, 2009b), Carretta & Bragaglia (2018), L13 from GIRAFFE spectra; Mészáros et al. (2020) from APOGEE spectra.

We discussed our findings also in connection with the ChM of NGC 6388 and other type-II GCs. About a third of giant stars in NGC 6388 are expected to be located in the region populated by red-RGB 'anomalous' stars that define the very nature of type-II GCs, according to the UV pseudo-colour diagram. However, no difference in metallicity is noticeable among these stars in NGC 6388 from our large sample studied with high resolution spectra. We conclude that either an intrinsic metallicity dispersion is not a necessary requisite for type-II GCs or NGC 6388 does not belong to this group. In the latter case, it would be necessary to understand the origin of the red-RGB stars on the ChM for this GC, as well as for M 15 and NGC 362, where an intrinsic metallicity dispersion is not found from a spectroscopic analysis of large samples of stars.

The homogeneous data presented in this paper also comprise the necessary first step for a complete characterisation of the chemistry of multiple stellar populations in NGC 6388, their relation with the cluster dynamics (e.g., rotation in the individual sub-populations) and its application in better defining the origin of this massive GC in the context of the GC population of the Milky Way. All of these issues will be explored in detail in a forthcoming paper.

Acknowledgements. We made extensive use of the ESO archive and we thank the personnel maintaining it and developing and applying the instrument pipelines. This research made use of observations made with the NASA/ESA *Hubble* Space Telescope obtained from the Space Telescope Science Institute, which is operated by the Association of Universities for Research in Astronomy, Inc. under NASA contract NAS 5-26555. We warmly thank Raffaele Gratton for useful discussion and Michele Bellazzini for sharing his code to measure intrinsic spreads. This research made use of the SIMBAD database (in particular Vizier), operated at CDS, Strasbourg, France, of the NASA Astrophysical Data System, of IRAF, and of TOPCAT (`http://www.starlink.ac.uk/topcat/`, Taylor 2005).

References

Alonso, A., Arribas, S., & Martinez-Roger, C. 1999, A&AS, 140, 261
Alonso, A., Arribas, S., & Martinez-Roger, C. 2001, A&A, 376, 1039
Asplund, M., Grevesse, N., Sauval, A. J., et al. 2009, ARA&A, 47, 481
Baumgardt, H., Hilker, M., Sollima, A., & Bellini, A. 2018, MNRAS, 482, 5138
Bekki, K., & Freeman, K. C. 2003, MNRAS, 346, L11
Bellazzini, M., Ibata, R. A., Chapman, S. C., et al. 2008, AJ, 136, 1147
Bragaglia, A., Carretta, E., Gratton, R. G., et al. 2001, AJ, 121, 327
Cardelli, J. A., Clayton, G. C., & Mathis, J. S. 1989, ApJ, 345, 245
Carretta, E. 2006, AJ, 131, 1766
Carretta, E. 2019, A&A, 624, A24
Carretta, E., & Bragaglia, A. 2018, A&A, 614, A109
Carretta, E., Gratton, R. G., Bragaglia, A., Bonifacio, P., & Pasquini, L. 2004, A&A, 416, 925
Carretta, E., Bragaglia, A., Gratton, R. G., et al. 2006, A&A, 450, 523

Carretta, E., Bragaglia, A., Gratton, R. G., et al. 2007a, A&A, 464, 967
Carretta, E., Recio-Blanco, A., Gratton, R. G., Piotto, G., & Bragaglia, A. 2007b, ApJ, 671, L125
Carretta, E., Bragaglia, A., Gratton, R. G., et al. 2009a, A&A, 505, 117
Carretta, E., Bragaglia, A., Gratton, R. G., & Lucatello, S. 2009b, A&A, 505, 139
Carretta, E., Bragaglia, A., Gratton, R. G., D'Orazi, V., & Lucatello, S. 2009c, A&A, 508, 695
Carretta, E., Bragaglia, A., Gratton, R. G., et al. 2010a, A&A, 516, A55
Carretta, E., Gratton, R. G., Lucatello, S., et al. 2010b, ApJ, 722, L1
Carretta, E., Bragaglia, A., Gratton, R. G., et al. 2010c, ApJ, 714, L7
Carretta, E., Bragaglia, A., Gratton, R. G., et al. 2010d, A&A, 520, A95
Carretta, E., Lucatello, S., Gratton, R. G., Bragaglia, A., & D'Orazi, V. 2011, A&A, 533, A69
Carretta, E., Bragaglia, A., Gratton, R. G., et al. 2013, A&A, 557, A138
Carretta, E., D'Orazi, V., Gratton, R. G., & Lucatello, S. 2014, A&A, 563, A32
Cordero, M. J., Pilachowski, C. A., Johnson, C. I., et al. 2014, ApJ, 780, 94
Dalessandro, E., Lanzoni, B., Ferraro, F. R., et al. 2008, ApJ, 677, 1069
D'Antona, F., & Caloi, V. 2004, ApJ, 611, 871
Forbes, D. A. 2020, MNRAS, 493, 847
Frischknecht, U., Hirschi, R., Pignatari, M., et al. 2016, MNRAS, 456, 1803
Gaia Collaboration (Brown, A. G. A., et al.) 2021, A&A, 649, A1
Gratton, R. G. 1988, Rome Obs. Preprint Ser., 29
Gratton, R. G., Carretta, E., Claudi, R., Lucatello, S., & Barbieri, M. 2003, A&A, 404, 187
Gratton, R. G., Lucatello, S., Bragaglia, A., et al. 2007, A&A, 464, 953
Gratton, R. G., Carretta, E., Bragaglia, A., Lucatello, S., & D'Orazi, V. 2010, A&A, 517, A81
Gratton, R. G., Bragaglia, A., Carretta, E., et al. 2019, A&ARv, 27, 8
Grevesse, N., & Sauval, A. J. 1998, Space Sci. Rev., 85, 161
Grevesse, N., Asplund, M., & Sauval, A. J. 2007, Space Sci. Rev., 130, 105
Han, S.-I., Lee, Y.-W., Joo, S.-J., et al. 2009, ApJ, 707, L190
Harris, W. E. 1996, AJ, 112, 1487
Hughes, J., Wallerstein, G., Covarrubias, R., & Hays, N. 2007, AJ, 134, 229
Husser, T.-O., Latour, M., Brinchmann, J., et al. 2020, A&A, 635, A114
Johnson, C. I., & Pilachowski, C. A. 2010, ApJ, 722, 1373
Johnson, C. I., Rich, M. R., Pilachowski, C. A., et al. 2015, AJ, 150, 63
Johnson, C. I., Caldwell, N., Rich, M. R., et al. 2017, ApJ, 836, 168
Kirby, E. N., Duggan, G., Ramirez-Ruiz, E., & Macias, P. 2020, ApJ, 891, L13
Kurucz, R. L. 1993, CD-ROM 13, Smithsonian AstrophysicalObservatory, Cambridge
Lanzoni, B., Mucciarelli, A., Origlia, L., et al. 2013, ApJ, 769, 107
Limongi, M., & Chieffi, A. 2018, ApJS, 237, 13
Lützgendorf, N., Gebhardt, K., Baumgardt, H., et al. 2015, A&A, 581, A1
Magain, P. 1984, A&A, 134, 189
Marino, A. F., Sneden, C., Kraft, R. P., et al. 2011, A&A, 532, A8
Marino, A. F., Milone, A. P., Karakas, A. I., et al. 2015, MNRAS, 450, 815
Marino, A. F., Milone, A. P., Renzini, A., et al. 2019, MNRAS, 487, 3815
Marino, A. F., Milone, A. P., Renzini, A., et al. 2021, ApJ, 923, 22
Massari, D., Koppelman, H. H., & Helmi, A. 2019, A&A, 630, L4
Mészáros, S., Masseron, T., García-Hernández, D. A., et al. 2020, MNRAS, 492, 1641
Milone, A. P., Piotto, G., Renzini, A., et al. 2017, MNRAS, 464, 3636
Minelli, A., Mucciarelli, A., Massari, D., et al. 2021, ApJ, 918, L32
Mucciarelli, A., Bellazzini, M., Ibata, R., et al. 2012, MNRAS, 426, 2889
Mucciarelli, A., Lapenna, E., Massari, D., et al. 2015, ApJ, 809, 128
Muñoz, C., Geisler, D., Villanova, S., et al. 2021, MNRAS, 506, 4676
Myeong, G. C., Vasiliev, E., & Iorio, G. 2019, MNRAS, 488, 1235
Nardiello, D., Libralato, M., Piotto, G., et al. 2018a, MNRAS, 481, 3382
Nardiello, D., Milone, A. P., Piotto, G., et al. 2018b, MNRAS, 477, 2004
Ortolani, S., Renzini, A., Gilmozzi, R., et al. 1995, Nature, 377, 701
Pasquini, L., Avila, G., Allaert, E., et al. 2000, Proc. SPIE, 4008, 129
Pfeffer, J., Lardo, C., Bastian, N., Saracino, S., & Kamann, S. 2021, MNRAS, 500, 2514
Piotto, G., Sosin, C., & King, I. R. 1997, in Advances in Stellar Evolution, eds. R. T. Rood, & A. Renzini (Cambridge: Cambridge Univ. Press), 84
Piotto, G., Milone, A. P., Bedin, L. R., et al. 2015, AJ, 149, 91
Raimondo, G., Castellani, V., Cassisi, S., Brocato, E., & Piotto, G. 2002, ApJ, 569, 975
Renzini, A., D'Antona, F., Cassisi, S., et al. 2015, MNRAS, 454, 4197
Roederer, I. U. 2011, ApJ, 732, L17
Siegel, M. H., Dotter, A., Majewski, S. R., et al. 2007, ApJ, 667, L57
Skrutskie, M. F., Cutri, R. M., Stiening, R., et al. 2006, AJ, 131, 1163
Sneden, C., Johnson, J., Kraft, R. P., et al. 2000, ApJ, L85
Sobeck, J. S., Kraft, R. P., Sneden, C., et al. 2011, AJ, 141, 175
Taylor, M. B. 2005, Astronomical Data Analysis Software and Systems XIV, 347, 29
Vasiliev, E., & Baumgardt, H. 2021, Catalogue of stars in Milky Way globular clusters from Gaia EDR3 (Zenodo), https://doi.org/10.5281/zenodo.4891252
Villanova, S., Geisler, D., & Piotto, G. 2010, ApJ, 722, 118
Wallerstein, G., Kovtyukh, V. V., & Andrievsky, S. M. 2007, AJ, 133, 1373
Worley, C. C., Hill, V., Sobeck, J., & Carretta, E. 2013, A&A, 553, A47
Yi, S., Demarque, P., & Oemler, A., Jr 1998, ApJ, 492, 480
Yong, D., Roederer, I. U., Grundahl, F., et al. 2014, MNRAS, 441, 3396